Electron collisions with BeH_2 below 20 eV

Journal Item

Electron collisions with BeH_2 below 20 eV

Ivan Sukuba*
Department of Nuclear Physics and Biophysics, Faculty of Mathematics, Physics and Informatics, Comenius University, 84248 Bratislava, Slovakia.

Jimena D. Gorfinkiel
School of Physical Sciences, The Open University, Walton Hall, Milton Keynes MK7 6AA, United Kingdom
(Dated: July 1, 2020)

We present calculations of electron scattering from BeH_2 using the R-matrix method. Integral and differential elastic and inelastic cross sections for energies up to 20 eV have been determined and the position and width (when possible) of shape and core-excited resonances is reported. The use of Gaussian, B-spline and mixed basis has been investigated. Results are compared with earlier calculations: it is shown that inclusion of both more target states and higher partial waves affect both the resonant behaviour at lower energies and the high-energy behaviour of the inelastic cross sections.

I. INTRODUCTION

Understanding and modelling electron induced processes in fusion plasma experiments are two of the key challenges for the successful achievement of energy-generating fusion reactors, ITER and DEMO, i.e. to show the viability and stability of sustained fusion plasma reaction [1, 2]. These electron induced processes are part of the plasma-wall interactions (PWIs), a complex interplay of various mechanisms, governing the relation between the materials of the inner walls of the reactor and the edge fusion plasma (the result of not fully magnetically contained fusion reaction) [3]. These walls, exposed to the fusion plasma ions (H^+, D^+, ...), change their physical and chemical properties as erosion caused by sputtering, transport and deposition develops. Damaged inner walls are not the sole result of these processes. Material is released into the edge plasma that could contaminate the main fusion reaction and decrease its effectiveness and stability.

The inner walls of the ITER reactor should be coated with beryllium (the first-wall material) and tungsten (divertor) [4]. Experiments with ITER-like reactor walls have already been performed at the Joint European Torus (JET) [5]. However, these experiments are being constantly complemented by modelling of these PWIs at different levels of theory, from quantum-chemical calculations [6] to molecular dynamics simulations [7] to use of numerous codes (like ERO[8] or EIRENE[9, 10]) for plasma and plasma-surface interaction modelling, to understand the principles of turbulence and transport mechanisms in the scrape-off layer or edge-plasma that cannot be fully explained by the experiments.

Electron impact excitation/ionization cross section data in collisions between atoms, molecules and electrons help quantify and clarify the interactions not only in fusion plasma but also, for example, in Astrochemistry. The main aim of this work is to improve the available electronic excitation cross section for BeH_2, one of the possible species eroded out of the first-walls besides Be and BeH [11]. The temperature in the edge and divertor plasma is 0.5-100 eV, so collisions with scattering energies in that range are of interest. Beryllium hydrides (deuterides) were confirmed by both experiment and modelling[12, 13] to be present in the fusion edge-plasma as the result of D^+ bombardment of the first-wall materials. Since then a lot of research has been performed in order to describe the properties of these molecules using experimental and theoretical means.

In contrast to BeH, BeH_2 is far less explored. Experimentally determined geometry and vibrational frequencies of the ground state were published only a few years ago [14]. A few publications are available concerning its potential energy surface, investigated using high-order *ab initio* methods, as well as its excited states and thermodynamic properties[15–18]. There are two publications concerning cross sections of BeH_2, one presenting electron impact ionization cross sections[19], the other covering lower energy scattering [20]. The latter work used the R-matrix approach as implemented in the commercial package Quantemol. There are a few works regarding BeH[21–23] that, interestingly, all used the R-matrix method for computing the cross sections. This method has been widely and successfully used [24] to describe both elastic scattering and electron induced electronic excitation in small and medium-size molecules (e.g. [25]) as well as small molecular clusters[26]. These calculations, however, can be of limited quality when the some of target electronic states of interest are very diffuse or for higher scattering energies, even below the ionization threshold. Both issues are related to the description of the free (continuum) electron in the R-matrix approach.

This paper has therefore another goal beyond improving earlier results for the electronic excitation cross section of BeH_2: we explore the advantages of using different continuum descriptions in R-matrix calculations. Until very recently, molecular R-matrix calculations used

* ivan.sukuba@fmph.uniba.sk

Gaussian type orbitals (GTOs) (also used to describe bound target orbitals) for the continuum description. However, recent developments of the UKRmol+ suite [27] have made it possible to use a mixed basis of GTOs and B-splines type orbitals (BTOs) and also a BTOs only basis. So far only one publication [21] has presented R-matrix electron-molecule scattering cross sections determined using a mixed continuum basis and no results have been reported using a BTO-only basis yet. We have performed a comparison of all 3 continuum basis types.

The method and the particular models used to calculate the excitation cross section are described in Sections II and III. The tests of various models are described in Sec. IV and the final results, comprising integral elastic and electronically inelastic cross sections as well as resonance parameters (Sec. V A) and differential cross section (Sec. V B) are discussed in Sec. V. Finally, we present some conclusions in Sec. VI.

II. METHOD

The R-matrix method, as implemented in the UKRmol+ suite [27] (release versions 2.0/2.0.2), was used to perform the scattering calculations. The method is based on discriminating the scattering problem spatially into an inner and outer regions. The boundary between these two regions is given by the R-matrix sphere with radius $r = a$. The time-independent Schrödinger equation is solved for the inner region wavefunction describing the target molecule and the target molecule plus scattering electron, using the standard —(non-relativistic) Hamiltonians. These calculations are independent of the scattering energy. The method requires that the target wavefunctions are fully contained within R-matrix sphere.

Subsequently, the energy-dependent R-matrix is built at the boundary and propagated to a large radius (in our calculations 100.0 a_0) where non-Coulombic potentials can be neglected and asymptotic expressions for the radial part of the wavefunction can be used. Matching to these functions[24], the K-matrices are determined. The eigenphase sums, cross section (via the S-matrix), and other scattering data can be obtained from the K-matrix.

As a consequence of this approach, the inner region equations have to be solved only once to produce multiple scattering energy-dependent solutions. Another advantage of the approach is the stability of propagating the wavefunction by using the R-matrix instead of direct numerical solutions.

In general, the $N + 1$-electron inner region wavefunction for a target with N electrons can be written as a linear combination of basis functions Ψ_k^{N+1} that have the *Close-Coupling* form:

$$\Psi_k^{N+1} = \mathcal{A} \sum_{i,j} a_{ijk} \Phi_i^N \gamma_{ij} + \sum_i b_{ik} \chi_i^{N+1} \qquad (1)$$

The Φ_i^N functions in the first term describe the target electronic states and the γ_{ij} are 'continuum' orbitals that represent the scattering electron and are the only non-zero terms at the R-matrix boundary. The χ^{N+1} functions in the second term, referred to as L^2 functions, describe short range correlation and polarization and are built from target orbitals; they are therefore fully contained within R-matrix sphere. The coefficients a_{ijk} and b_{ik} are determined by diagolinazation of the N+1 Hamiltonian [24] matrix in the inner region. The operator $\mathcal{A}$ secures the proper antisymmetrization of the wavefunction.

A. Target and scattering models

The overall performance of the R-matrix method depends on the models chosen to describe the target molecule and the scattering process (N+1 electron system). The target model is chosen in such a way that the quality of the quantum-chemical description of the molecule and its computational cost are balanced. The UKRmol+ suite is capable of using molecular orbitals generated by an external quantum chemistry package provided in the form of a MOLDEN file. Orbitals produced by the self-consistent field Hartree-Fock (HF) method or the complete active space self-consistent-field (CASSCF) approach (in order of the computational feasibility and amount of the electron correlation described) are normally used.

Another important choice is that of the atomic basis set which should guarantee a good description of the molecular orbitals as well as its suitability within the UKRmol+ suite, e.g. the orbitals have to be confined within the R-matrix sphere. Too diffuse and/or robust basis sets could either leak outside the R-matrix sphere or cause numerical instabilities that could result, for example, in nonphysical resonances.

The scattering model describes the interplay between the target molecule and the scattering electron. The quality of the continuum description (the continuum orbitals used) is one key factor. The other is the amount of short-range correlation-polarization that is described. The simplest model is called static exchange (SE) and uses HF orbitals and a HF description of the target ground state with no polarization allowed.

The static exchange plus polarization (SEP) model is also based on the HF method, but improves the description of the interaction with the impinging electron by allowing one of the valence electrons to be promoted to one of a subset of virtual orbitals.

Both models mentioned so far can only describe elastic scattering and will only describe well shape resonances. The close-coupling (CC) model involves the inclusion of electronic excited states of the molecule in Eq. (1), though only those energetically closely-coupled, to allow a more flexible treatment of the scattering process. Consequently, the target model must describe both the ground and some electronically excited states of the tar-

get. Balance between the target and N+1 calculations can be achieved using a complete active space configuration interaction (CAS-CI) approach to the target description. In this case, the L^2 functions can be written as:

$$\chi_i^{N+1}(CC) = (core)^{N_c}(CAS)^{N-N_c+1} \quad (2)$$

$$\chi_i^{N+1}(CC) = (core)^{N_c}(CAS)^{N-N_c}(virtual)^1 \quad (3)$$

N_c is the number of core electrons. The second type of configurations described by the above equations is only required when the target is highly polarizable and should be used with care as it can unbalance the calculation. In that case, there is no *a priori* correct choice of the number of virtual orbitals to use.

B. Representation of the continuum

In the inner region, the continuum electron is described by a set of 'continuum' orbitals, γ_{ij} in Eq. (1), which have been commonly constructed from GTOs centred on the centre of mass of the system [24]. GTOs are not very well suited to representing the highly-oscillating behaviour of the true continuum functions both over an extended radial range and when higher values of the kinetic energy of the scattering electron need to be considered. Therefore their use restricts both the size of R-matrix spheres that can be used and the collision energies that can be treated.

To overcome this limitation, the re-engineered version of the molecular R-matrix codes (UKRmol+) allows for use of B-spline type orbitals (BTOs): one can use only GTOs, only BTOs or a mix of both to represent the continuum orbitals. In the latter case, the GTOs are chosen to describe the continuum accurately up to a radius a_{GTO} and the BTOs cover the range between a_{BTO} (the radius where B-splines start) and the R-matrix radius.

In order to obtain orthogonal orbitals (required by our R-matrix implementation) first a Gramm-Schmidt orthogonalization to the target orbitals is performed. Then, a symmetric orthogonalization is used: in this step, the orbitals with eigenvalues of the overlap matrix lower than some deletion threshold are deleted from the basis. Typically, for GTOs the threshold value is $\sim 10^{-7} - 10^{-9}$ depending on the R-matrix radius (and lower in quadruple precision calculations [28]). Higher deletion thresholds ensure avoidance of linear dependence and numerical instabilities, but reduce the quality of the continuum description. The typical value of the deletion threshold for B-splines is higher, usually $10^{-4} - 10^{-5}$ (for mixed basis these higher deletion thresholds are also used). Further details on how the deletion thresholds are determined and the characteristics of the BTO basis can be found elsewhere [27].

As a final note regarding the continuum description we indicate that when a BTO-only continuum is used, the UKRmol+ suite allows calculations l_{max}=8 and higher. This is significant when higher scattering energies are explored: even for non-polar targets like BeH_2, where the partial wave expansion is expected to converge for a few of them, the effect of including l =7, 8 partial waves is noticeable at higher energies, particularly for the inelastic cross sections.

III. PRESENT CALCULATIONS

A. Target model

BeH_2 is a 6 electron molecule with a linear geometry and an experimental Be-H bond of 1.326 Å(2.506 a_0) [14] in its ground state, and thus no dipole moment. In the equilibrium ground state configuration the $1\sigma_g$ $1\sigma_u$ and $2\sigma_g$ orbitals are doubly occupied. In the present calculations we have used a bond length of 1.332 Å(2.513 a_0) obtained from calculations with the coupled-cluster approximation (CC2) method using the aug-cc-pVTZ basis set [17] (Calculations using these two geometries yielded practically identical cross sections, but the CAS-CI energies are slightly lower for the latter). In addition, as is standard in quantum chemistry calculations, we have used the Abelian D_{2h} point group (rather than the $D_{\infty h}$). This means that, in the paper, we shall mostly use the irreducible representations of the former point group. The ionization threshold is estimated to be 11.93 eV [19].

In order to find the best target and scattering models for describing the electronic excitation of BeH_2 an analysis of various models was performed. The CASSCF method and (aug)-cc-pVXZ basis sets, X=D,T and Q, were tested to obtain accurate target orbitals. The orbitals were generated with MOLPRO [29]. For comparison, the coupled-cluster approximation (CC2) using multiresolution analysis (MRA)[17] and equation of motion – coupled clusters singles and doubles (EOM-CCSD/cc-pVTZ) calculations [20] of excited states were used.

In the state-averaged CASSCF calculations, one frozen core orbital (the $1\sigma_g/1a_g$) was used and the 4 remaining electrons were allowed to occupy the 14 lowest lying orbitals (2-5 a_g, 1-2 b_{3u}, 1-2 b_{2u}, 1 b_{1g}, 1-3 b_{1u}, 1 b_{2g}, 1 b_{3g} and no a_u), i.e. a (4,14) active space was tested using the above-mentioned basis sets. Several state-averaging options (including different sets of states) were tested for the different basis sets tried.

The SA-CASSCF calculation with cc-pVDZ basis set, averaging the lowest ^1A_g, ^3A_g,$^3B_{2g}$ and $^3B_{3g}$ states with identical weight was chosen as the best balance between computational cost and quality of the target description [30]. Adding diffuse functions improved only higher excited states, but required the use of a larger R-matrix radius and thus more computational resources. The comparison of ground state energy and vertical excitation energies for the lowest states obtained using the best target model with two atomic basis sets is summarized in Table I. Also, further investigation of use of the valence triple and quadruple zeta basis sets showed only slight improvement for cc-pVXZ and almost no change for aug-

TABLE I. Ground state energy in Hartree and vertical excitation energies in eV for first 21 excited states of BeH_2 using the SA-CASSCF approach and the (aug)-cc-pVDZ basis sets. Earlier theoretical data is also listed: (a) EOM-CCSD[20], (b) CC2-MRA[17] and (c) CAS-CI[20].

State		Current		Other		
D_{2h}	$D_{\infty h}$	cc-pVDZ	aug-cc-pVDZ	(a)	(b)	(c)
^1A_g	$^1\Sigma_g^+$	-15.831	-15.825			-15.78
$^3B_{2g}+{}^3B_{3g}$	$^3\Pi_g$	6.225	6.053	6.147		6.15
$^1B_{2g}+{}^1B_{3g}$	$^1\Pi_g$	6.611	6.481	6.548	6.808	6.48
$^3B_{2u}+{}^3B_{3u}$	$^3\Pi_u$	7.162	7.023	7.046		7.19
$^3B_{1u}$	$^3\Sigma_u^+$	8.565	8.919	8.588		8.79
$^1B_{2u}+{}^1B_{3u}$	$^1\Pi_u$	9.026	8.943	8.717	8.904	9.08
^3A_g	$^3\Sigma_g^+$	10.090	9.113	9.744		10.71
$^1B_{1u}$	$^1\Sigma_u^+$	10.767	9.350		9.415	11.36
^1A_g	$^1\Sigma_g^+$	10.923	10.329		9.982	11.14
$^3B_{1g}$		12.528	12.271			12.23
$^1B_{1g}$		13.168	12.807			
^3A_u		13.219	12.817			
^3A_u		13.470	13.233			
^1A_g		13.490	11.254			
$^3B_{1u}$		13.602	10.806			
$^3B_{1u}$		14.189	11.599			
^1A_g		14.355	13.112			
^1A_u		14.412	14.182			
$^3B_{2u}+{}^3B_{3u}$		14.907	15.507			
$^3B_{2g}+{}^3B_{3g}$		16.082	15.594			
^3A_g		16.084	11.128			
$^3B_{1u}$		16.555	13.314			

cc-pVXZ basis sets in comparison with the corresponding data in the table. It is for this reason that we chose to use the compact basis set (cc-pVDZ), that requires less computational effort. The agreement with earlier calculations is overall good.

The transition dipole moments and permanent quadrupole moments for the lowest 9 states calculated with this basis are shown in Table II. Agreement with Gupta *et al.* is reasonable for the first 3 excited states (note, however, that the signs of some of the components of the quadrupole moment are different; we attribute this to the use of different software and we are confident our results are correct). For higher states, the differences are significant and are either related to a different description of the excited states in our calculations or, again, the use of different software (Quantemol uses the UKRmol suite).

B. Scattering models

In order to find the best scattering model for describing both elastic and inelastic scattering from BeH_2, a number of continuum bases (GTO only, mixed and BTO only) and orthogonalization deletion thresholds were tested. Convergence of the partial wave expansion (by performing calculations for different l_{max}) was also checked.

TABLE II. Transition dipole moments (with the ground state) and permanent quadrupole moment components (in brackets), in atomic units, for the 9 lowest states of BeH_2 from our SA-CASSCF calculation using the cc-pVDZ basis sets. The results of Gupta *et al.* [20] are also listed.

state			
D_{2h}	$D_{\infty h}$	This work	[20]
^1A_g	$^1\Sigma_g^+$	(3.66)	(3.4541)
$^3B_{2g}/{}^3B_{3g}$	$^3\Pi_g$	(-2.81, -3.64)	(-3.1708, 3.3643)
$^1B_{2g}/{}^1B_{3g}$	$^1\Pi_g$	0.0, (-3.13, 3.84)	0.0, (-3.5048, 3.4926)
$^3B_{2u}/{}^3B_{3u}$	$^3\Pi_u$	(-1.73, -3.75)	(-2.1279, 3.3201)
$^3B_{1u}$	$^3\Sigma_u^+$	(-2.71)	(-1.7107)
$^1B_{2u}/{}^1B_{3u}$	$^1\Pi_u$	1.36, (-0.98, -3.88)	-1.4674, (-0.0927, 3.7184)
^3A_g	$^3\Sigma_g^+$	(-0.58)	(0.0872)
$^1B_{1u}$	$^1\Sigma_u^+$	-1.19 (-2.28)	1.3713, (0.0267)
^1A_g	$^1\Sigma_g^+$	(-2.89)	(-1.8157)

For the target model using the cc-pVDZ basis set (and SA-CASSCF orbitals) an R-matrix radius of 15 a_0 was sufficient. Most of these test calculations included 14 states in the close-coupling expansion (these are D_{2h} states) 13 of which have excitation thresholds below the ionization threshold for this basis set. This model was used to test the different approaches to describing the continuum.

The exponents for the GTO basis set in GTO-only calculation were those for 15 a_0; maximum angular momenta l_{max}=4,5,6 were tested as well as deletion thresholds down to 10^{-11}. The mixed GTO/BTO continuum calculations were performed with $a_{GTO} = 10a_0$ and $a_{BTO} = 4a_0$ and a much higher deletion threshold of 10^{-4} was applied.

As a test, the radius of 6 a_0 for a_{GTO} was used for the mixed basis (only $l_{max} = 4$) and the results were hardly affected. The B-splines were constructed of 20 functions of order 9 with the first two removed due to discontinuity of their derivative in both types of calculation, the mixed GTO/BTO and BTO-only. For BTO-only runs both parameters, a_{GTO} and a_{BTO}, are simply set to 0. Here one can use a bigger range of angular momenta: in this work BTO-only calculations with l_{max} up to 8 were performed.

In the following section, we will show results for a range of these scattering models. The aim here is two-fold: on one hand, we were looking for the most accurate model possible for the BeH_2 cross sections. On the other, we wanted to investigate the performance of the mixed and BTO-only basis sets as these have only been used for a small number of R-matrix calculations so far [27]. Our aim was to obtain a good continuum description up to 20 eV.

Since BeH_2 has no dipole moment, no additional Born correction is required.

IV. TESTS OF MODELS AND CONVERGENCE

Fig. 1 shows the integral elastic cross sections for calculations using the compact basis set, $a = 15\ a_0$, 14 target states in the CC expansion and GTO-only, mixed GTO/BTO and BTO-only basis sets with $l_{max} = 5$.

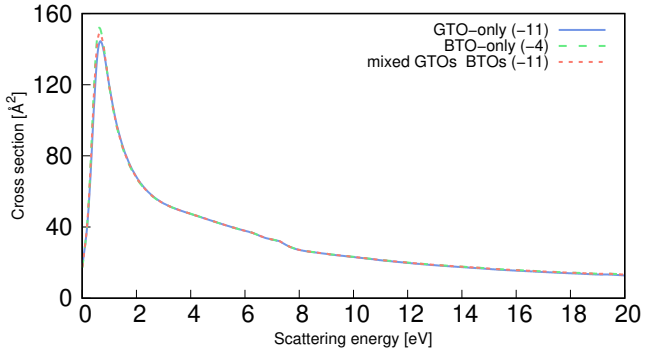

FIG. 1. Integral elastic cross section calculated with the compact basis set, $a = 15\ a_0$ and 14 target states in the close coupling expansion using the three different types of continuum indicated in the figure (the numbers n in brackets correspond to the exponent in the deletion threshold, 10^n, used).

The results are extremely similar, showing that for this radius all 3 types of continuum basis produce elastic results of a similar quality. One way of ascertaining the quality of the continuum description before proceeding to a full scattering calculation is to calculate the eigenphase sum for free potential scattering: as this quantity should be zero, the smaller the value, the better the continuum basis being used. Our results seem to indicate that continua that produce larger values than recommended [27] are still good enough: for the GTO-only basis the eigenphase sums (for each irreducible representation) are between 0.05 and 0.12 for 20 eV (whereas for the other two basis is of the order of 10^{-3}). It also shows that differences of 2 orders of magnitude in the free potential scattering eigenphase sums have little effect: for the GTO-only basis the eigenphase sum is as big as of 2-4$\times$ 10 $^{-3}$ for most irreducible representations below 10 eV while for the other 2 types of continuum basis it is around 2 orders of magnitude smaller.

All this calculations describe a peak in the cross section (corresponding to a resonance of $^2\Pi_u$ symmetry) at a very similar scattering energy: $\sim$ 0.65 eV, with a cross section maximum of $\sim$ 150 Å^2. The relative deviation is $\sim$4% with the BTO-only basis giving the highest peak.

The effect of increasing l_{max} on the integral elastic cross section is small, as can can be seen in Figs. 2 and 3 in which the details of the tail and the peak, respectively, are depicted. The additional angular momenta contribute only slightly to the overall convergence of the elastic cross section. In both cases, it is clear that use of the GTO-only basis produces the most different results.

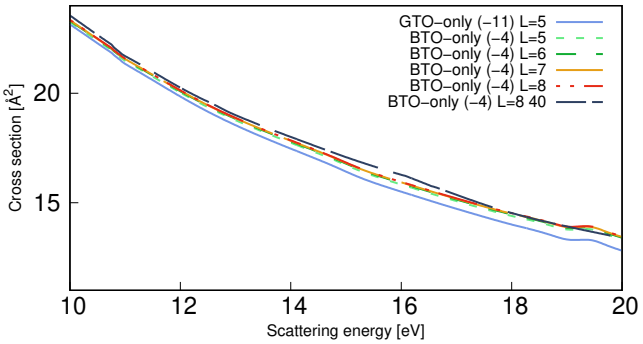

FIG. 2. Integral elastic cross section - detail of the tail. Calculations using different types of continuum indicated in the figure (the numbers n in brackets correspond to the exponent in the deletion threshold, 10^n, used) and 14 states, unless otherwise indicated. The maximum partial wave is also indicated (as L) in the panel.

Figs. 2 and 3 also show the comparison of results obtained including different number of states in the CC expansion. Increasing the number of target states does not affect the cross section above 4 eV: the only noticeable effect is the removal of a small kink at around 19.5 eV (see Fig. 2).

It is clear from Fig. 3 that increasing the number of states produces a shift of the peak in the cross section (for the same continuum basis and l_{max}) to lower energies: from around 0.65 eV down to 0.59 eV. Increasing the number states improves the description of polarization effects; it is well known that the position of shape resonances, like the low-energy $^2\Pi_u$ resonance of BeH_2, is strongly dependent on the polarization description [24, 31]. One way of estimating the contribution of the target states to the quality of this description is to calculate the spherical polarizability of the target using the sum-over-states formula and those states included in the CC expansion. The experimental value for BeH_2 is 29.29 a_0^3 [32] whereas these models predict values between $9-12\ a_0^3$: for the cc-pVDZ basis set the values for 14, 25 and 40 states are, respectively, 9.88, 9.88 and 11.62 a_0^3; increasing the number of states to 96 increases this value to 13.99 a_0^3. It seems, therefore, that inclusion of pseudostates in the close-coupling expansion [33] would be required to converge the polarizability as is the case for many targets. We note that use of the aug-cc-pVDZ basis set improves the polarizability description, but not significantly: for 40 states the value is 12.75 a_0^3.

Figure 3 includes the results of Gupta *et al* [20]: the shape of the cross section is the same for energies above 0.8-0.9 eV but different below, where the effect of the resonance is most significant. Attempts to reproduce Gupta's results (i.e. using their best model: 6-31G* basis set, Hartree-Fock orbitals, a (4,6) active space for the CAS-CI calculations and 25 electronic states in the CC expansion, l_{max}=4 and the C_{2v} point group) lead to a

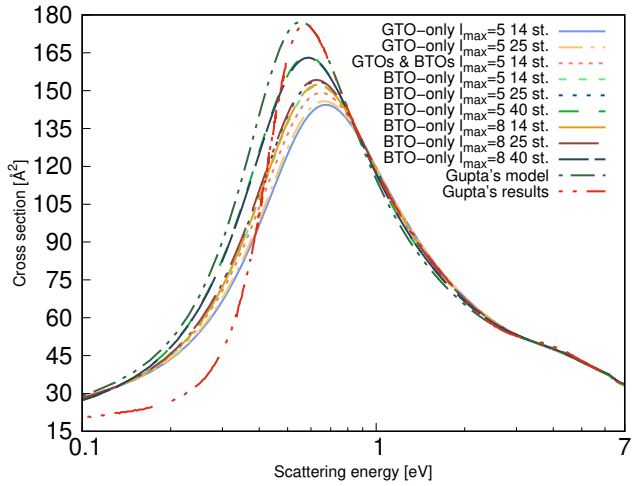

FIG. 3. Detail of the lowest resonance in the elastic cross section for the continuum bases, l_{max} and number of states indicated in the figure. 'Gupta's model' corresponds to our calculations using the parameters of Gupta *et al.* (see text for more details) whereas 'Gupta's results' corresponds to their calculation.

cross section with the resonance peak at the same energy and with a nearly identical height. However, the behaviour of the cross section below the energy for the maximum differed, with our results (using their model) producing a cross section that decreased more slowly. We ascribe this to differences to the software used: at these very low energies we believe differences may be due to the (now) correct treatment of the transition moments that model the electron-molecule interaction in the outer region.

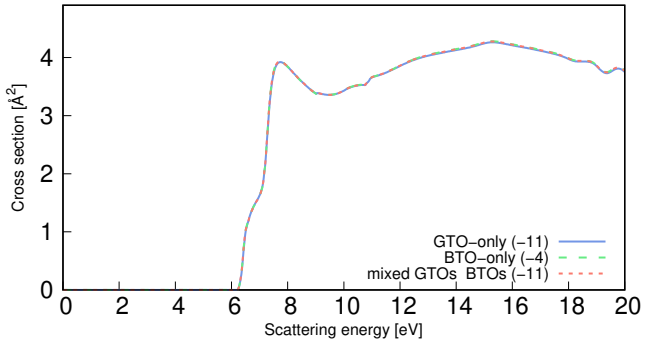

FIG. 4. Total (summed over all excited states included in the calculation) integral electronic excitation calculated using the three different types of continuum basis sets and 14 target states for the compact basis set; l_{max}=5 in all calculations. The numbers n in brackets correspond to the exponent in the deletion threshold, 10^n, used.

The total inelastic cross section, calculated with 14 states, is shown in Fig. 4. Again, the difference between all three tested continuum basis types is negligible. However, the size of the cross section above 9 eV is strongly affected by the additional angular momenta: the effect is clearly visible in Fig. 5, with l_{max}=8 giving a cross section that is 16% bigger than that given by l_{max}=4 at 15 eV and around 30% bigger at 20 eV. One can also see that as l_{max} increases, the effect of adding an extra partial wave decreases.

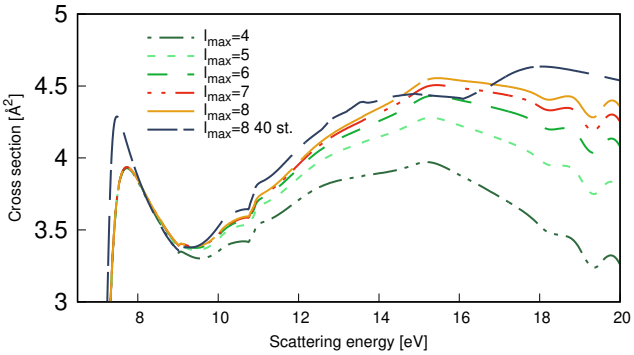

FIG. 5. Effect of the inclusion of more partial waves on the total (summed over all excited states) integral electronic excitation cross sections- detail of the tail. Calculations performed using BTOs only and 14 target states unless otherwise stated.

The effect of including more states in the CC expansion is illustrated in Fig. 6: both the higher energy range and the region just below 8 eV show noticeable differences. State number 15 (in D_{2h}) has a threshold of around 13.2 eV while that of state 26 is around 16 eV: it is at these energies where the total inelastic cross sections calculated using different number of states show changes in behavior with respect to one another. The shape of the cross section below 8 eV is given, at least partially, by a resonant contribution. As discussed above, inclusion of more states improves the description of polarization effects and therefore shifts resonant peaks to slightly lower energies.

V. THE FINAL SCATTERING RESULTS

Inspecting the previous results, it was found that the scattering model with BTO-only continuum and maximum angular momentum of l_{max}=8 including 40 target states represents our best model for description of electron scattering from BeH_2. The results for that model are plotted and discussed in this section.

Figure 7 shows both our total and momentum transfer (MTCS) cross sections. The lowest energy resonance is visible in both; the MTCS results are very similar to those of Gupta *et al.* (also plotted) except for the lower-energy behaviour of the resonance; this difference was also observed for the integral elastic cross section.

Figure 8 shows our cross sections for excitation into the lowest 5 states of BeH_2, together with those of Gupta *et*

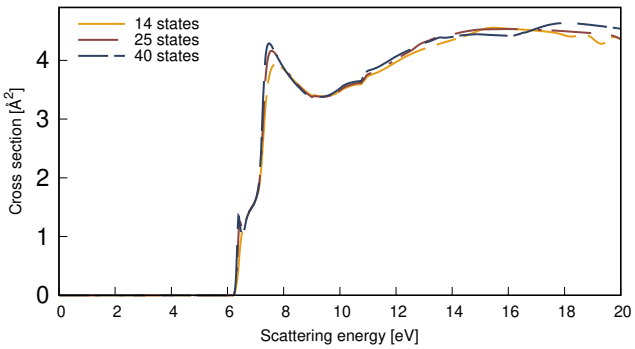

FIG. 6. Total (summed over all excited states included in the calculation) inelastic cross section. Comparison of calculations with different number of states indicated in the figure, using a BTO-only continuum basis set (deletion threshold of 10^{-4}) and l_{max}=8. Note the appearance of a spike just above threshold for the calculations with 25 and 40 states.

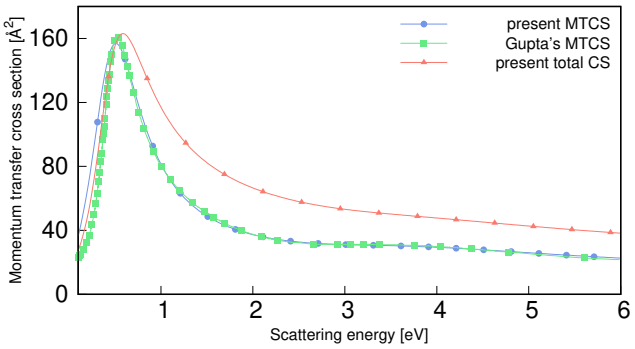

FIG. 7. Momentum transfer (MTCS) and total (CS) cross section for calculations with our best model. Comparison with Gupta's MTCS results.

al; all transitions, except that to the $^1\Pi_u$ state are dipole forbidden. The general trend of the cross sections is similar, but clear differences are visible, particularly at the lower range of the energy scale in the figure. At higher energies, our cross sections for excitation into the $^3\Sigma_u^+$ and $^1\Pi_u$ states are somewhat smaller, while those of Gupta *et al* are a bit bigger. This differences could be due to the inclusion of more states in the CC expansion in our calculations (40 in ours, versus 25 in theirs) or a combination of this and other effects (i.e. improved representation of the continuum, inclusion of higher partial waves). To test this, the effect of changing the number of states in the state-to-state inelastic cross sections is shown in Fig. 9: increasing the number of states from 14 to 40 leads to higher maxima for the $^3\Pi_g$ and $^3\Pi_u$ cross sections. The other noticeable difference is the appearance of a threshold peak in the $^3\Pi_g$ cross section when more states are included, as highlighted above. Otherwise, the differences are small up to 15 eV, with the 40-state cross sections being slightly bigger for all final states; this demonstrates that the increased number of states is not the main effect causing the differences between our and Gupta *et al*'s results at higher energies.

Finally, we note that Gupta *et al*'s cross section for excitation into the $^3\Pi_g$ state is smaller than ours in the region of the maximum but shows similar structure linked to the presence of 3 resonances, whereas the one for excitation into the $^3\Pi_u$ state is noticeably smaller. All other cross sections increase smoothly with energy in this range.

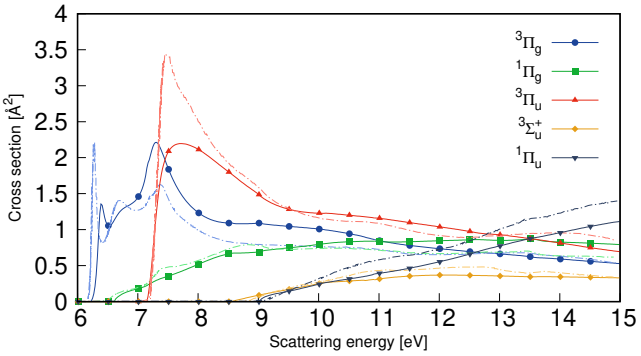

FIG. 8. State-to-state electronic excitation cross sections from the ground state: the state being excited is indicated in the figure. Our results (full lines) and those of of Gupta *et al* (dashed lines) are plotted using the same colour-coding.

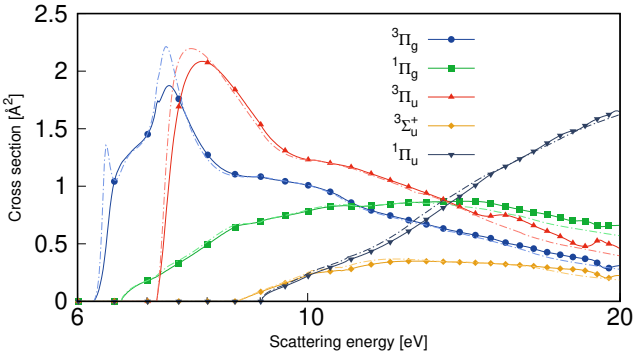

FIG. 9. State-to-state electronic excitation cross sections from the ground state: the state being excited is indicated in the figure. Calculations are for 14 (solid) and 40 (dashed) states included in the CC expansion.

A. Resonances

Table III summarizes the resonances found in our calculations; we have not attempted to identify resonances above 10 eV. These resonance were identified using both a visual inspection of the eigenphase sum and time-delays [34] and the program RESON [35] that fits the former

to the well known Breit-Wigner formula. For degenerate states, the position and width is slightly different for different symmetries: this can be attributed to slightly different modelling of the polarization effect for different symmetries.

TABLE III. Resonance position (E) and width (Γ, when available) obtained from our best model. When result are different for the different D_{2h} components of the degenerate $D_{\infty h}$ states, values for both are listed. Results from Gupta *et al.* are also included, with the resonance widths in brackets.

Symm.		E (eV)	Γ(eV)	Gupta[20]
D_{2h}	$D_{\infty h}$			
$^2B_{2u}/^2B_{3u}$	$^2\Pi_u$	0.419	0.55	0.45(0.40)
^2A_g	$^2\Sigma_g^+$	3.5	-	
$^2A_u/^2B_{1u}$	$^2\Delta_u$	≃6.21	v. narrow	
$^2A_u/^2B_{1u}$	$^2\Delta_u$	6.39/6.36	0.088/0.13	6.24(0.02)
$^2B_{1u}$	$^2\Sigma_u^+$	6.74	-	
$^2A_g/^2B_{1g}$	$^2\Delta_g$	7.33/7.24	0.50/0.48	7.44(0.38)/7.37(0.40)
$^2B_{2g}/^2B_{3g}$	$^2\Pi_g$	8.3-8.4	-	

We note first that the lowest shape resonance (of $^2\Pi_u$ symmetry) is located at 0.42 eV (this value, obtained by RESON, is the same for both D_{2h} contributions to the resonance) whereas the peak in the elastic cross section is seen at rather higher energies: this is not entirely surprising as non-resonant contributions to the cross section can shift the resonance peak from where it appears in the eigenphase sum.

We find four more resonances than those identified previously [20]. Agreement for those resonances identified in both works is reasonable if the resonance identified as Δ_g by Gupta *et al.* is assigned Δ_u character. Also, we believe those described by Gupta *et al.* as Σ_g^+ and Σ_g^- at 7.44 and 7.37 eV actually correspond to a Δ_g degenerate resonance: our calculation places each of the D_{2h} components of this resonance around 0.1 eV apart but with very similar widths. It is possible, however, that these are actually two resonances of Σ_g^+ and Σ_g^- symmetry.

The additional resonances are: one of Σ_g^+ symmetry at 3.5 eV, a very narrow one of Δ_u character around 6.21 eV, one of Σ_u^+ symmetry at 6.74 eV and a Π_g at around 8.3-8.4 eV. Our attempts to run an identical calculation to that of Gupta *et al.* did not show resonances that could be correlated to these last two, something that we ascribe to the use of a different basis set and poorer scattering model overall.

In order to investigate the character of the resonances, we have also performed SE and SEP calculations using the same basis set (cc-pVDZ) to generate HF orbitals, a BTO only continuum basis and partial waves up to $l_{max} = 4$; an R-matrix radius a=15 a_0 was used for the SE calculation, but a=18 a_0 was needed for the SEP ones. In the SEP calculation, all virtual orbitals were used for the L^2 function. The elastic cross section obtained in both models, together with the contribution of each irreducible representation (excluding B_{3g} and B_{3u} that are identical to B_{2g} and B_{2u} respectively) are plotted in Fig. 10; the SE cross section is extremely similar to that of Gupta *et al.*, but not identical because the basis sets used are different. For completeness, we have also plotted the elastic cross section and the contributions to it from our best CC model.

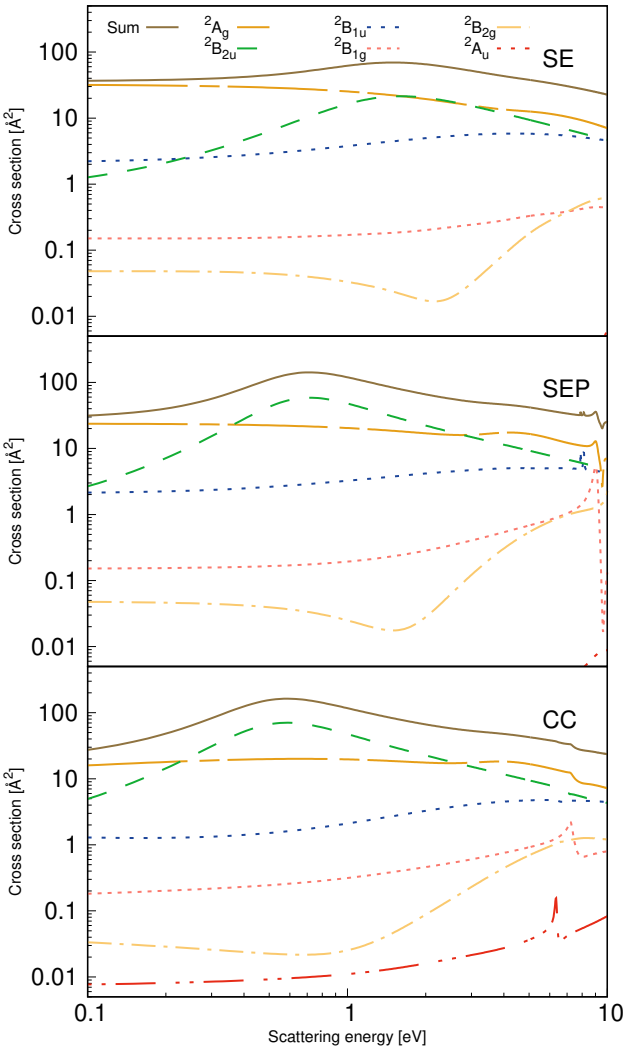

FIG. 10. Symmetry decomposition of the elastic cross section for static exchange (SE), static exchange plus polarization (SEP) models and our best close-coupling (CC) model as indicated in the panels. The total (summed over all symmetries) elastic cross section is also plotted for all models. Note the non-continuous cross section scale in the SEP and CC panels.

The $^2\Pi_u$ shape resonance is clearly visible in the $^2B_{2u}$ contribution for all models as expected. Less obvious, but still visible (and visible in the corresponding eigenphase sum, not presented here) is a broad peak in the ^2A_g SE contribution at around 4-6 eV and at somewhat lower energies in the SEP results. This is clearly linked to the ^2A_g resonance we identify in our CC results at 3.5 eV, demonstrating its shape character. No other resonant

features are visible in the SE results; those present in the SEP ones above 7-8 eV are likely to be non-physical pseudoresonances characteristic of this model in R-matrix calculations [24].

The CC results show a small, but clear peak above 7 eV in the ^2A_g and $^2B_{1g}$ contributions (also visible in the summed cross section): this corresponds to the $^2\Delta_g$ resonance we identify at 2.2-7.3 eV that would therefore seem to have some contribution of shape character.

Of the resonances identified by us, it is clear the first two are therefore shape resonances: the lowest one corresponds to the electron attaching to the LUMO orbital (of π_u symmetry) and the second one to an attachment into the LUMO+1 of σ_g symmetry. The rest are very likely of core-excited character (or mixed shape core-excited character in the case of the $^2\Delta_g$ one) and, except for the very narrow resonance of Δ_u symmetry and the feature around 8.3-8.4 eV, appear around 0.2 eV above the first three excited states; this and their width points at a core-excited shape character.

Going back to the CC results in more detail, the eigenphase sum of A_g symmetry shows a broad structure centred around 3.5 eV that correlates with an enhancement of the A_g contribution to the elastic cross section (at somewhat higher energies) and a wide structure in the time-delay, centred around 3.3 eV with a width of 3.3 eV; RESON does not fit it as a resonance, but this may be due to the fact that it's quite wide.

In addition, we identify a very narrow resonance of Δ_u symmetry. The corresponding features are visible in the eigenphase sum and time-delay, particularly for the A_u symmetry, but are too narrow to fit, so no exact position or width can be extracted. This is a narrow resonance, of Feshbach character, that only becomes sufficiently well described when a bigger number of excited states are included in the CC expansion, improving the overall description of the collision. We note that a test further improving the description of polarization effects by including in the calculation configurations of the type (3) provided a qualitatively similar picture of the resonance spectrum (same character and resonance ordering) with the resonances shifted downwards by less than 0.1 eV.

Similarly, there's a clear peak in the B_{1u} contribution to the total inelastic cross section at around 6.74 (not present for the A_u symmetry) that looks resonant in nature but does not correspond to a clear structure in the eigenphase sum. Another structure is visible at 8.3-8.4 eV in eigenphase sum for the B_{2g} and B_{3g} symmetries, broad and too small to be fitted by RESON but with a corresponding peak in the B_{2g} and B_{3g} contributions to the electronic excitation cross sections. The time-delay shows a broad structure centred around 8.5 eV, truncated by the presence of a threshold at 8.56 eV thus making it very hard to fit in order to determine its width and accurate position.

The Π_u resonance is visible in the elastic, total and MTCS cross sections. The threshold peak in the $^3\Pi_g$ cross section (see Fig. 8) corresponds to the Δ_u resonance around 6.3-6.4 eV; the Σ_u^+ resonance is visible as a shoulder at slightly higher energies and the maximum of this cross section is due to the Δ_g resonance around 7.3 eV.

B. Differential cross section

The elastic differential cross sections (DCS) obtained with our best model using the program DCS [36] are plotted in Figure 11 for selected energies up to 15 eV. For all plotted energies, the DCS shows a minimum that shifts to lower angles (from 105° to 85°), except for the 3 eV DCS: its peak appears slightly above 110°. An inspection of DCS for other energies shows that the dependence of the minimum with scattering energy is more complex: up to around 2 eV the minimum shifts towards bigger angles, it then stabilizes and from around 3 eV starts to move again to smaller angles. The lowest minima below 4.5 eV occur between 2.2-2.8 eV at ∼110° as can be seen in Figure 12. For higher energies the minimum moves to smaller angles: around 80° above 8 eV.

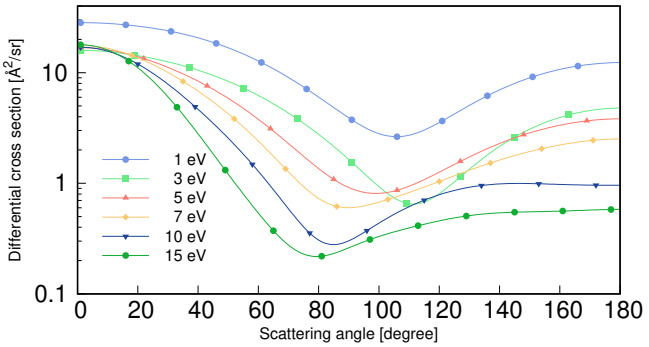

FIG. 11. Elastic differential cross section for calculations with our best model for the scattering energies indicated in the panel.

Again, with the exception of the 3 eV DCS, the size of the DCS decreases for increasing energy in the whole angular range: the differences in the forward scattering angles are negligible above ∼3 eV, but the effect on the backwards scattering is significant. Our DCS for 1,3, and 5 eV are very similar to those of Gupta *et al.*, but not for higher energies. Those for 7 and 10 eV are very different: our results for 25 states (the highest number of states used by Gupta *et al.*) are almost identical to those for 40 states. We attribute these differences to the fact that Gupta *et al.* used the original version of POLYDCS [37], that calculates the DCS using K-matrices. The K-matrix has the dimension of open channels at a given energy; in CC calculations, this means that the size of the K-matrix increases as the scattering energy increases and more inelastic channels become open. Use of the CC K-matrix in POLYDCS implies neglecting the coupling to the inelastic channels: this effect will get bigger as the kinetic

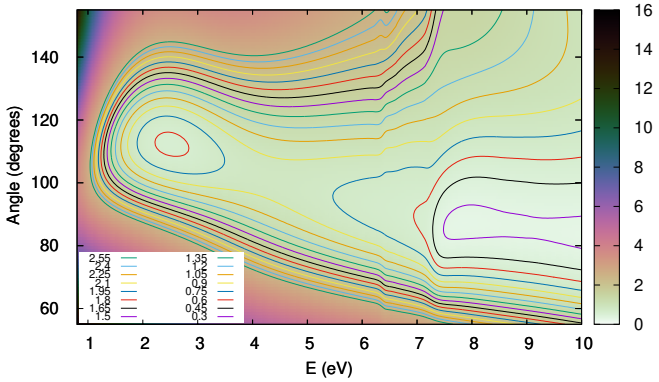

FIG. 12. Elastic differential cross section calculated with our best model as a function of scattering energy and angle. The colour scale on the right indicates the size of the DCS in the whole range shown, whereas the contour lines provide a clearer view of its minima.

energy increases. This problem can be circumvented if T-matrices are used in the calculation [38]. When we repeat our DCS calculation using an adapted version of POLYDCS [37] that uses the T-matrices, the results are very similar to those calculate with the DCS program.

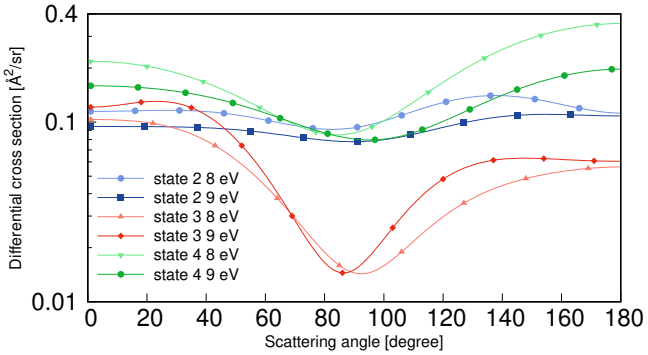

FIG. 13. State-to-state inelastic differential cross section calculated at 8 and 9 eV with our best model for the three lowest excited states of BeH_2: $^3\Pi_g$ (state 2), $^1\Pi_g$ (state 3), $^3\Pi_u$ (state 4).

Finally, Figure 13 shows the inelastic differential cross sections for excitation into the first three ($^3\Pi_g$, $^1\Pi_g$, $^3\Pi_u$) states of BeH_2 for a couple of energies. As expected, the cross sections for the triplet states are weakly dependent on the scattering angles, whereas the differential cross sections for excitation into the singlet state shows a minimum between 85° and 95° for both energies.

VI. CONCLUSIONS

We have used the state-of-the-art UKRmol+ suite to determine elastic and inelastic integral and differential cross sections for electron scattering from BeH_2. For the model used in the final calculations, that involved the cc-pVDZ basis set, all three type of continuum bases (GTO-only, BTO-only and mixed GTO-BTO) provide a similar quality of description up to 20 eV. Use of the UKRmol+ suite has enabled us to include higher angular momenta in the partial wave expansion (l_{max}=8): this was shown to have a significant effect in the total inelastic cross section that, at 20 eV, is about 30% bigger than when l_{max}=4 is used.

The calculated integral elastic cross section is dominated by a low energy shape resonance that also dominates the momentum transfer cross section. The total inelastic cross section is fairly constant in the energy range 8-20 eV. Inclusion of more states in the close-coupling expansion has a small effect on the total inelastic cross section above 15 eV or so, but also affects the lower energy region, where the cross section is dominated by a resonant peak that shifts to slightly lower energies when more states are taken into account. We attribute this to an improvement in the description of the correlation-polarization when more states are included.

The elastic differential cross sections have been calculated using close-coupling T-matrices (rather than K-matrices). They show a decreasing dependency on angle as the scattering energy increases, becoming rather flat above 130° for scattering energies of 10 eV. The differential cross section for excitation into the lowest three excited states show the expected isotropic behaviour for the triplet states, but a stronger angular dependence for the singlet state.

Two shape and 5 core-excited resonances have been identified in our calculations, some of which agree with earlier R-matrix results [20].

VII. ACKNOWLEDGEMENTS

This project has received funding from the European Union's Horizon 2020 research and innovation programme under grant agreement No 692335. We are grateful to Drs. Jakub Benda and Zdeněk Mašín for advice on the use of mixed and BTO-only continuum basis sets.

[1] R. Pitts, S. Carpentier, F. Escourbiac, T. Hirai, V. Komarov, A. Kukushkin, S. Lisgo, A. Loarte, M. Merola, R. Mitteau, A. Raffray, M. Shimada, and P. Stangeby, Journal of Nuclear Materials **415**, S957 (2011).

[2] S. Brezinsek, J. W. Coenen, T. Schwarz-Selinger, K. Schmid, A. Kirschner, A. Hakola, F. L. Tabares, H. J.

Van Der Meiden, M. Mayoral, M. Reinhart, E. Tsitrone, T. Ahlgren, and E. al., Nuclear Fusion **57**, 116041 (9pp) (2017).
[3] J. Roth, E. Tsitrone, A. Loarte, T. Loarer, G. Counsell, R. Neu, V. Philipps, S. Brezinsek, M. Lehnen, P. Coad, C. Grisolia, K. Schmid, K. Krieger, A. Kallenbach, B. Lipschultz, R. Doerner, R. Causey, V. Alimov, W. Shu, O. Ogorodnikova, A. Kirschner, G. Federici, and A. Kukushkin, Journal of Nuclear Materials **390–391**, 1 (2009).
[4] G. Federici, Physica Scripta **T124**, 1 (2006).
[5] F. Romanelli and J. E. T. E. Contributors, Nuclear Fusion **53**, 104002 (2013).
[6] A. Allouche and C. Linsmeier, Journal of Physics: Conference Series **117**, 12002 (2008).
[7] E. Safi, C. Björkas, A. Lasa, K. Nordlund, I. Sukuba, and M. Probst, Journal of Nuclear Materials **463**, (2015).
[8] D. Borodin, A. Kirschner, S. Carpentier-Chouchana, R. A. Pitts, S. Lisgo, C. Björkas, P. C. Stangeby, J. D. Elder, A. Galonska, D. Matveev, V. Philipps, and U. Samm, Physica Scripta **T145**, 014008 (2011).
[9] A. Taroni, G. Corrigan, R. Simonini, J. Spence, and S. Weber, Journal of Nuclear Materials **220-222**, 1086 (1995).
[10] D. Reiter, Journal of Nuclear Materials **196-198**, 80 (1992).
[11] S. Brezinsek, A. Widdowson, M. Mayer, V. Philipps, P. Baron-Wiechec, J. W. Coenen, K. Heinola, A. Huber, J. Likonen, P. Petersson, M. Rubel, M. F. F. Stamp, D. Borodin, J. P. P. Coad, A. G. G. Carrasco, A. Kirschner, S. Krat, K. Krieger, B. Lipschultz, C. Linsmeier, G. F. F. Matthews, and K. Schmid, Nuclear Fusion **55**, 63021 (2015).
[12] C. Björkas, K. Vörtler, K. Nordlund, D. Nishijima, and R. Doerner, New Journal of Physics **11**, 123017 (2009).
[13] M. F. Stamp, K. Krieger, and S. Brezinsek, Journal of Nuclear Materials **415**, S170 (2011).
[14] A. Shayesteh, K. Tereszchuk, P. F. Bernath, and R. Colin, Journal of Chemical Physics **118**, 3622 (2003).
[15] J. Koput and K. A. Peterson, The Journal of Chemical Physics **125**, (2006).
[16] J. Hinze, O. Friedrich, and A. Sundermann, Molecular Physics **96**, 711 (1999).
[17] J. S. Kottmann and F. A. Bischoff, Journal of Chemical Theory and Computation **13**, 5956 (2017).
[18] I. Sukuba, A. Kaiser, S. Huber, J. Urban, and M. Probst, Journal of Molecular Modeling **23** (2017), 10.1007/s00894-017-3362-4.
[19] T. Maihom, I. Sukuba, R. Janev, K. Becker, T. Märk, A. Kaiser, J. Limtrakul, J. Urban, P. Mach, and M. Probst, The European Physical Journal D **67**, 1 (2013).
[20] D. Gupta, M.-Y. Song, H. Choi, D.-C. Kwon, K. L. Baluja, and J. Tennyson, Journal of Physics B: Atomic, Molecular and Optical Physics **52**, 65204 (2019).
[21] D. Darby-Lewis, Z. Mašín, and J. Tennyson, Journal of Physics B: Atomic, Molecular and Optical Physics **50**, 175201 (2017).
[22] C. Björkas, D. Borodin, A. Kirschner, R. K. Janev, D. Nishijima, R. Doerner, and K. Nordlund, Journal of Nuclear Materials **438**, S276 (2013).
[23] R. Celiberto, R. K. Janev, and D. Reiter, Plasma Physics and Controlled Fusion **54**, 35012 (2012).
[24] J. Tennyson, Phys. Rep. **491**, 29 (2010).
[25] A. Loupas, K. Regeta, M. Allan, and J. D. Gorfinkiel, The Journal of Physical Chemistry A **122**, 1146 (2018), https://doi.org/10.1021/acs.jpca.7b11865.
[26] A. Sieradzka and J. D. Gorfinkiel, The Journal of Chemical Physics **147**, 034303 (2017), http://dx.doi.org/10.1063/1.4993946.
[27] Z. Mašín, J. Benda, J. D. Gorfinkiel, A. G. Harvey, and J. Tennyson, Computer Physics Communications **249**, 107092 (2020).
[28] A. Loupas and J. D. Gorfinkiel, The Journal of Chemical Physics **150**, 064307 (2019).
[29] H.-J. Werner, P. J. Knowles, G. Knizia, F. R. Manby, and M. Schütz, WIREs Comput. Mol. Sci. **2**, 242 (2012).
[30] The effect of including the ^3A_g state in the averaging is rather small; in fact, several other choices of states gave similar results, provided the 3 lowest energy states were included.
[31] Z. Mašín and J. D. Gorfinkiel, The Journal of Chemical Physics **137**, 204312 (2012).
[32] NIST Computational Chemistry Comparison and Benchmark Database , "Nist standard reference database number 101," (2018).
[33] J. D. Gorfinkiel and J. Tennyson, J. Phys. B: At. Mol. Opt. Phys. **37**, L343 (2004).
[34] K. Smith, *The calculation of atomic collision processes* (Wiley-Interscience, New York, 1971) Chap. 4.
[35] J. Tennyson and C. J. Noble, Comput. Phys. Commun. **33**, 421 (1984).
[36] Z. Mašín, "DCS: a program to generate orientation-averaged DCS for electronically elastic and inelastic collisions," (2018), https://gitlab.com/Masin/DCS.
[37] N. Sanna and F. A. Gianturco, Computer Phys. Comm. **114**, 142 (1998).
[38] Z. Mašín, *Resonance formation in electron collisions with pyrimidine-like targets*, Ph.D. thesis, The Open University (2012).